

Supporting Information

From -20 °C to 150 °C: Lithium Secondary Battery with a Wide Temperature Window via Manipulated Competitive Decomposition in Electrolyte Solution

Tianle Zheng^{‡a,b}, Jianwei Xuong^{‡b}, Bingying Zhu^b, Xiaotang Shi^b, Ya-Jun Cheng^{*b},
Hongbin Zhao^{*a}, Yonggao Xia^{*b,c}

a. Department of Chemistry, College of Sciences. Shanghai University, 200444,
Shanghai. P. R. China

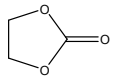
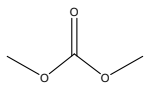
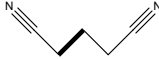
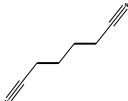
b. Ningbo Institute of Materials Technology & Engineering, Chinese Academy of
Sciences, 1219 Zhongguan West Rd, Ningbo, 315201, Zhejiang Province, P. R.
China

c. Center of Materials Science and Optoelectronics Engineering, University of
Chinese Academy of Sciences, 19A Yuquan Rd, Shijingshan District, Beijing
100049, P. R.

[‡] T. Zheng and J. Xiong contributed equally to this work.

E-mail: chengyj@nimte.ac.cn, hongbinzhao@shu.edu.cn, and xiayg@nimte.ac.cn

Table S1. List of physical properties of dinitrile solvents and common carbonate solvents used in lithium electrolyte solutions¹⁻⁴

Sample	Structure	ϵ	H (cp)	T_m (°C)	T_b (°C)	T_f (°C)	T_{auto} (°C)
EC		89	2@40°C	35	244	15	465
DMC		3	0.7	3	90	18	458
Acetonitrile	CH₃CN	37	0.3	-48	81	2	523
Glutaronitrile		37	5.3	-29	287	113	
Adiponitrile		30	6.1	1	295	163	550

Note. ϵ is dielectric constant, η is viscosity, T_m is melting point, T_b is boiling point, T_f is flash temperature, and T_{auto} is auto-ignition temperature.

Table S2. First cycle performance of the Li/LTO cells cycled at various rates at different temperatures

Temperature (°C)	rate	Charge capacity (mAh/g)	Discharge capacity (mAh/g)	CE%
-40	0.2 C	32.51	23.80	136.6-
	-	-	-	-
-20	1 C	95.45	128.44	74.3
	-	-	-	-
30	1 C	139.70	156.90	89.0
	5 C	93.00	104.10	89.3
100	1 C	168.84	217.90	77.5
	5 C	171.34	220.03	77.9
120	1 C	130.59	226.30	57.7
	5 C	178.47	228.86	78.0
150	1 C	164.02	310.91	52.8
	5 C	165.15	285.61	57.8

Table S3. First cycle performance of the Li/LFP cells cycled at 0.2 C or 1 C at different temperatures

Temperature (°C)	rate	Charge capacity (mAh/g)	Discharge capacity (mAh/g)	CE%
-20	0.2 C	173.52	133.87	77.2
	1 C	64.46	41.05	63.7
30	0.2 C	162.63	152.34	93.7
	1 C	147.4	140.8	95.5
100	0.2 C	217.90	168.84	77.5
	1 C	196.15	152.80	77.9
120	0.2 C	262.50	144.9	55.2
	1 C	238.65	138.2	57.9
150	-	-	-	-
	1 C	311.11	146.67	47.1

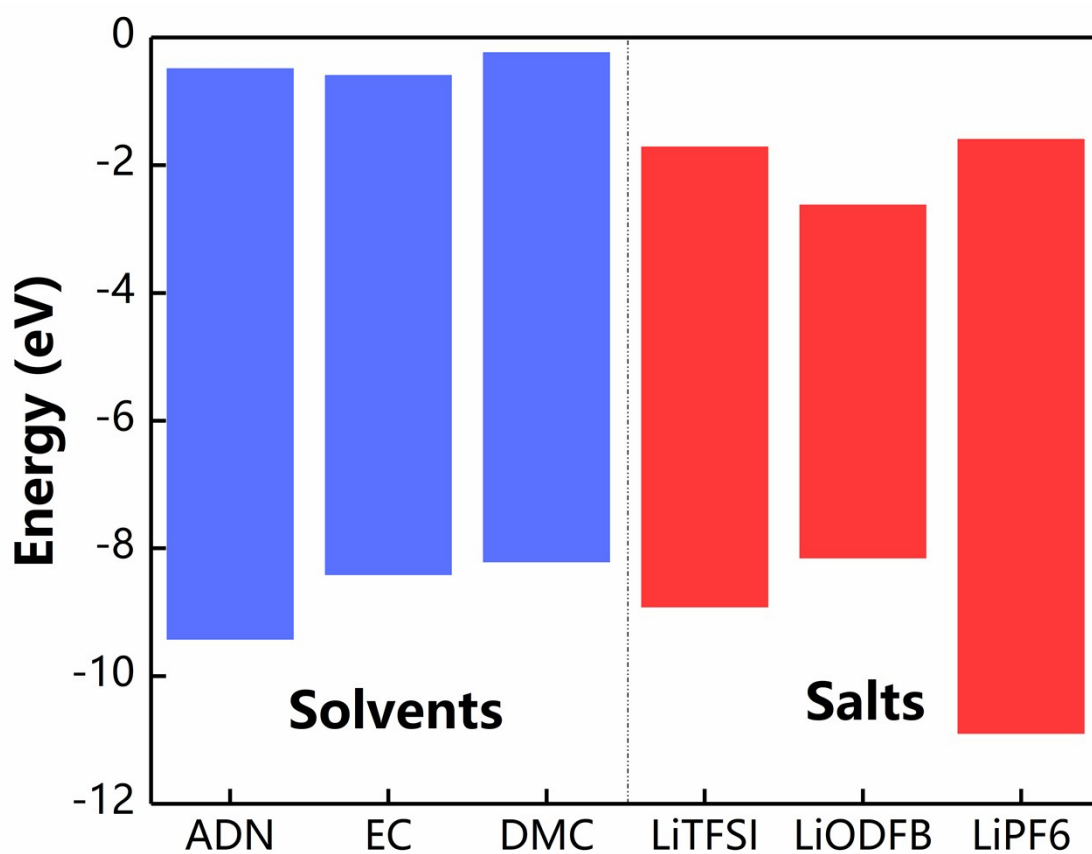


Figure S1. The HOMO and LUMO of different solvents and lithium salts in electrolytes.

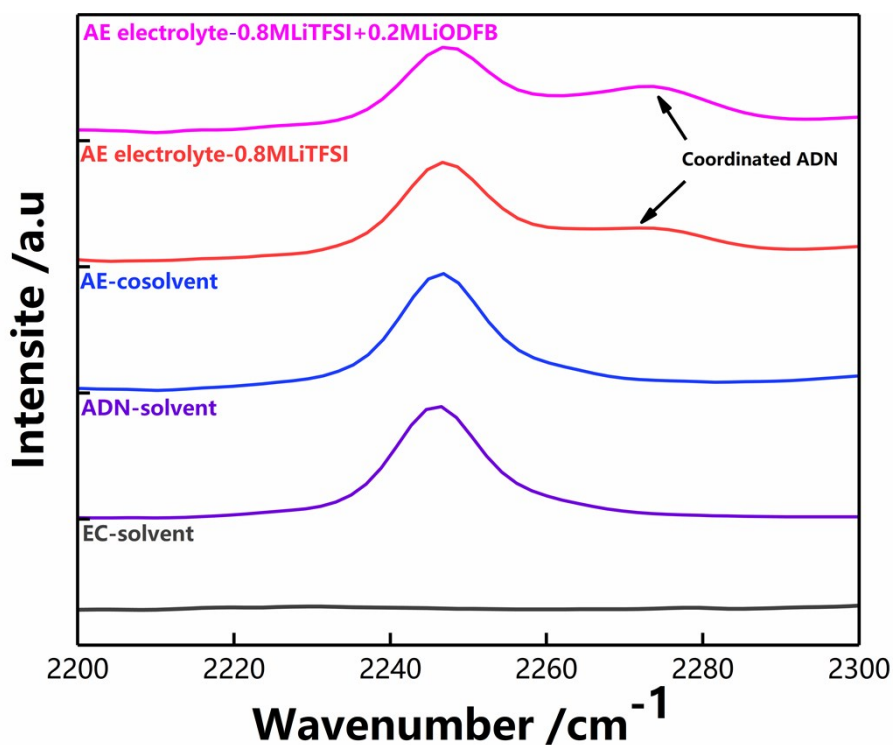


Figure S2. FTIR spectra of different solvents and electrolyte solutions.

ADN is chosen as a co-solvent for EC solvent due to its high flashing point, low viscosity, and good thermal stability. As demonstrated in **Figure S1**, pure ADN and AE co-solvent (ADN:EC=1:1) both show a typical vibration band at 2247 cm^{-1} corresponding to the nitrile bond. With addition of 0.8 M of LiTFSI or 0.2 M of LiODFB, a new peak appears at 2274 cm^{-1} , which is attributed to lithium ions solvated with ADN molecules. Besides, the addition of 0.8 M of LiTFSI and 0.2 M of LiODFB increases the height of the solvation peak. It means that the concentration of lithium ions is increased because both LiTFSI and LiODFB can increase the solvation degree of the lithium ion.

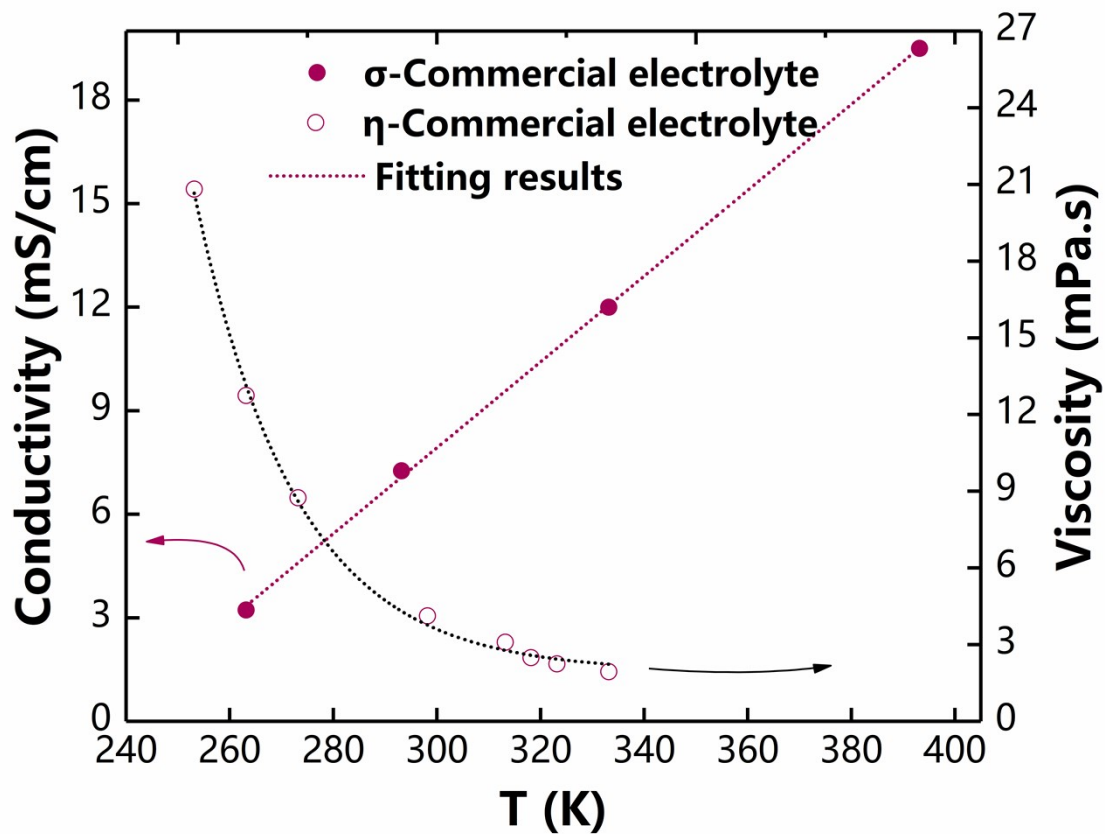


Figure S3. Evolution of the viscosity (η , left) and conductivity (σ , right) of the AE electrolyte solution (1M LiPF_6 in the EC/DMC co-solvent with the volume ratio of 3:7) as a function of temperature.

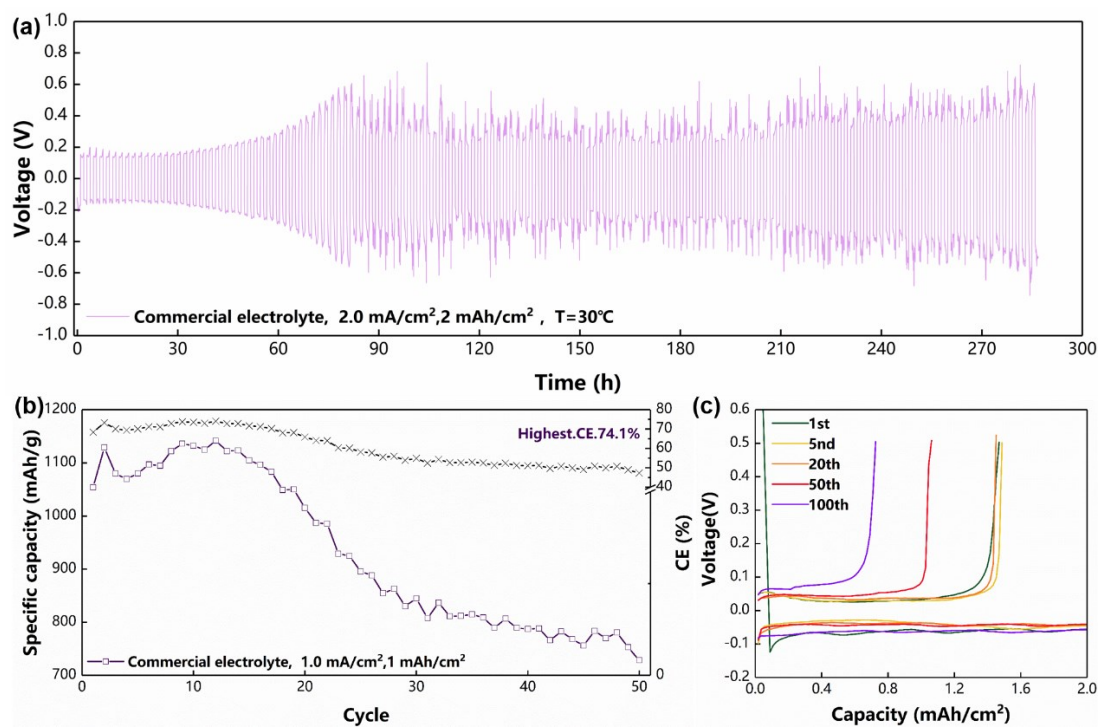


Figure S4. Electrochemical performance of the Li/Li cells with the commercial electrolyte solution (1 M of LiPF_6 in EC/DMC (3/7, v./v.)) at 30 °C (a); The CE of Li metal plating/stripping over 50 cycles in commercial electrolyte solution at 30 °C (b); voltage profiles of the cell using commercial electrolyte solution with current density of 1.0 mA/cm² at 30 °C (c).

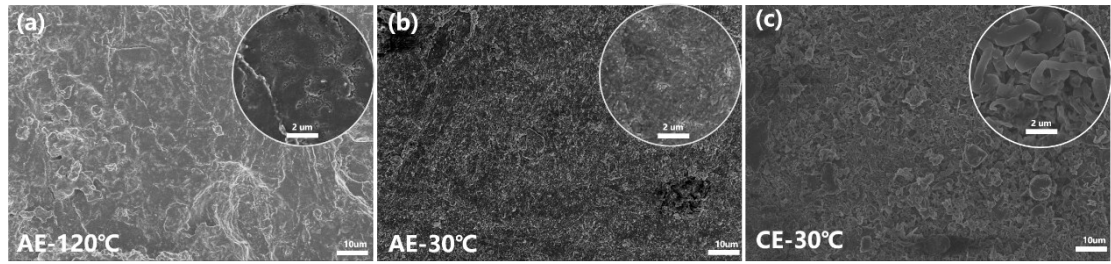


Figure S5. Morphologies of the Li metal anode in the AE co-solvent electrolyte solution cycled at (a) 120 °C and (b) 30 °C and in commercial electrolyte solution at 30 °C (c).

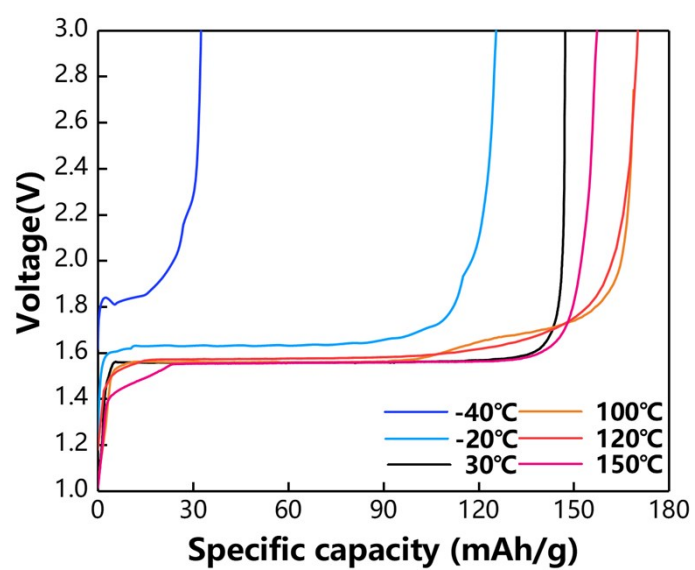


Figure S6. The first charge profiles of the Li/LTO cells with the AE electrolyte solution at different temperatures.

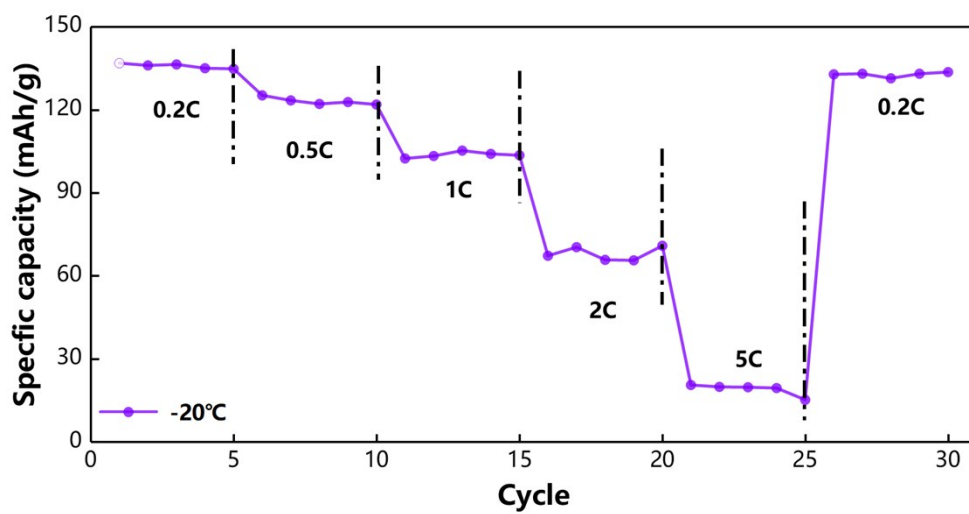


Figure S7. Rate performance of the Li/LTO cells with the AE electrolyte solution at -20 °C.

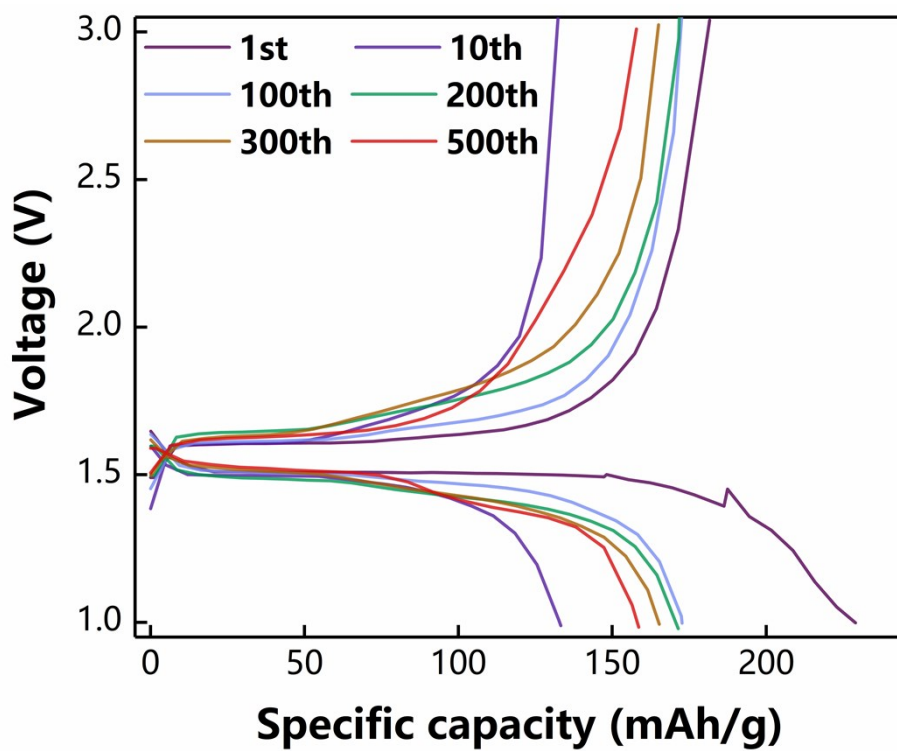


Figure S8. Charge-discharge curves of the Li/LTO cell with AE electrolyte after different cycles at 120 °C.

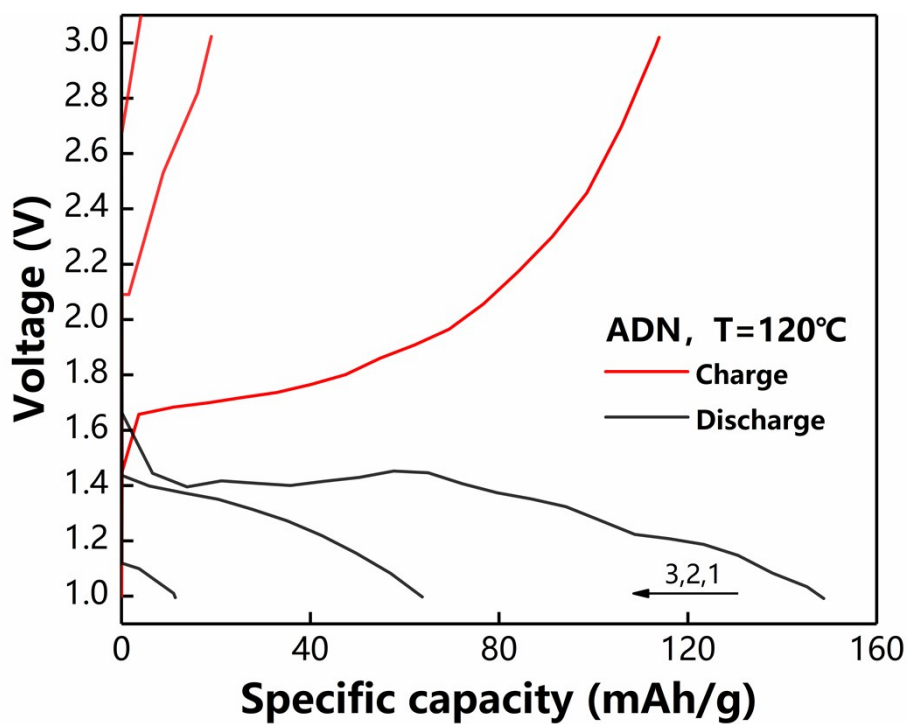


Figure S9. Charge-discharge curves of the Li/LTO cell with the ADN single solvent electrolyte solution after 3 cycles at 120 °C.

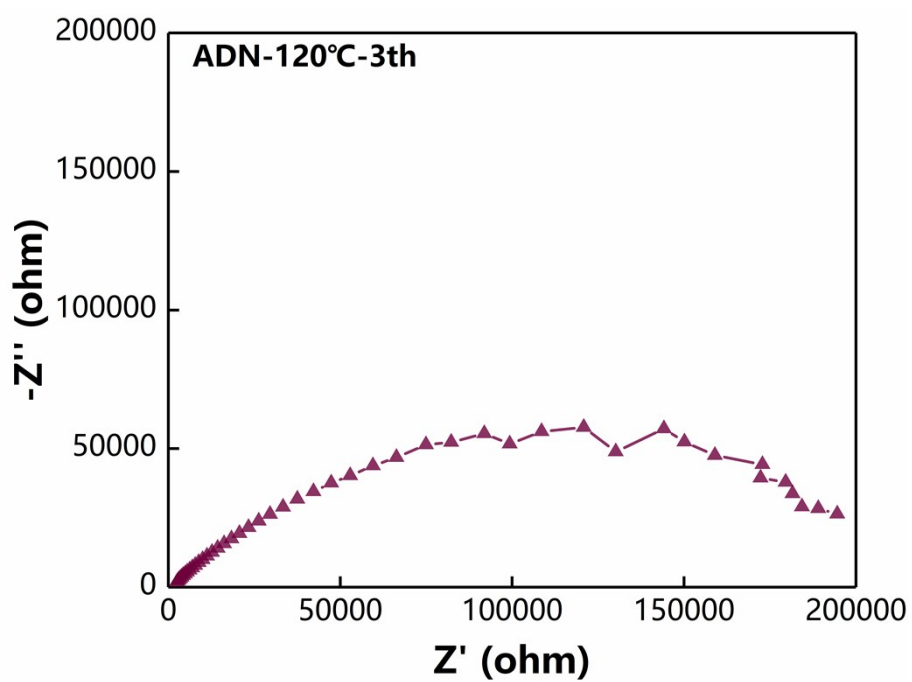


Figure S10. Impedance spectra of the Li/LTO cells cycled with the ADN single solvent electrolyte solution.

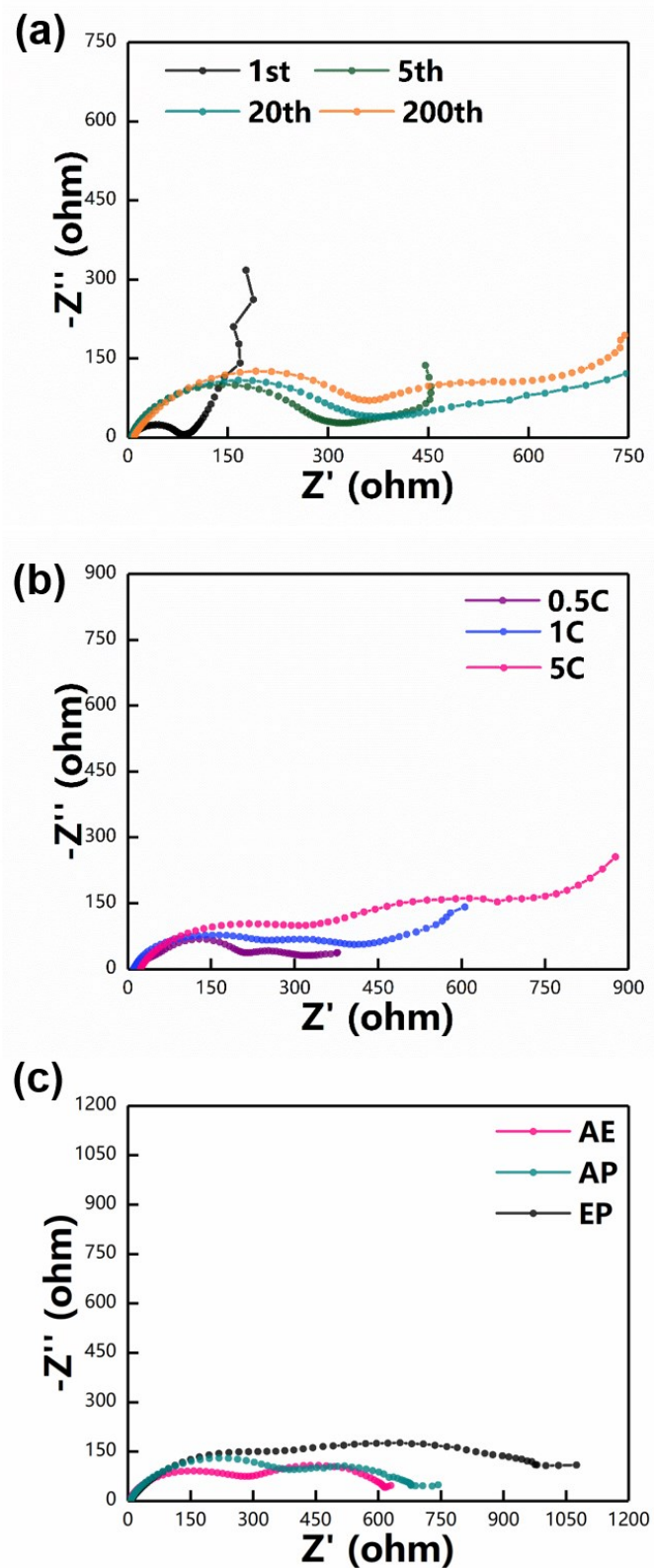


Figure S11. Impedance spectra of the Li/LTO cells cycled at 100 °C after different cycles with the AE electrolyte at rate of 1 C (a), after 200 cycles with the AE electrolyte at different rates (b), and after 200 cycles with different co-solvent electrolytes (AP: ADN/PC, EP: EC/PC) at rate of 1 C (c).

At high temperature, the interface impedance of the battery with AE electrolyte increases with the increase cycling. **(Figure S11a)** And a higher current density results in a higher impedance of interface of the cells. **(Figure S11b)**

Additionally, for investigating the differences among various co-solvent electrolytes, the Li/LTO cells with AE, AP ($V_{ADN} : V_{PC}=1:1$) and EP ($V_{EC} : V_{PC}=1:1$) co-solvent electrolytes have assembled, and **Figure S11c** shows the cells with AE electrolyte harbors the lower interface impedance, indicating the AE electrolyte could promote to form a SEI possesses a high conductivity.

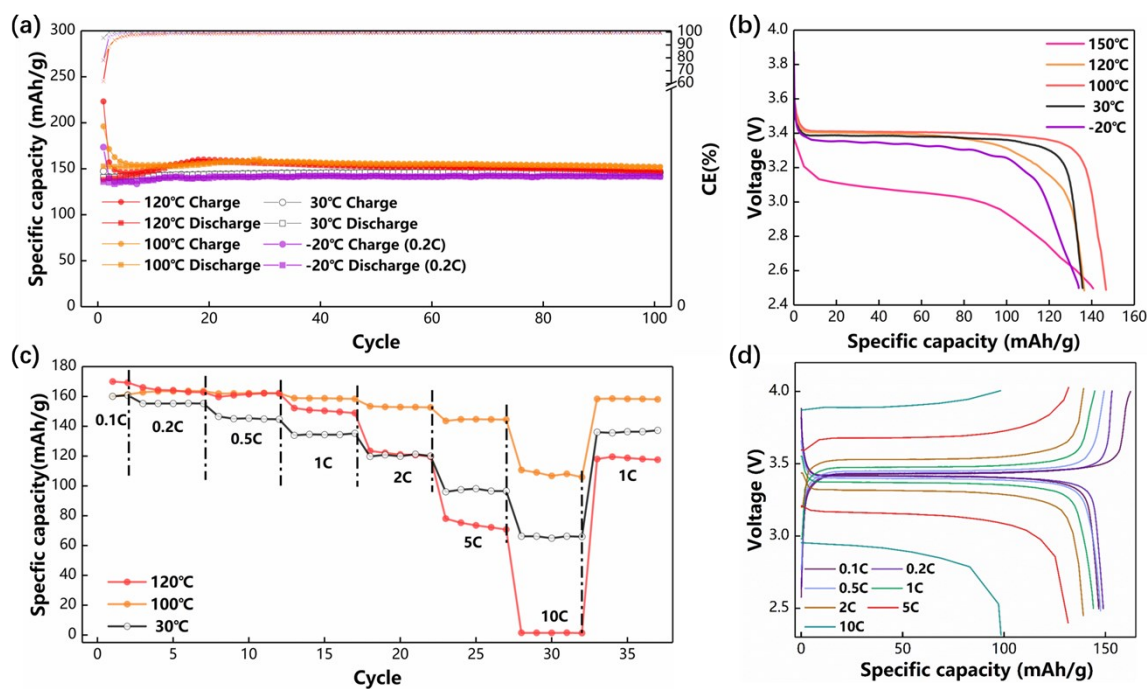


Figure S12. (a) Cycling performance of the Li/LFP cells with the AE electrolyte at 1 C or 0.2 C in the voltage range of 2.5 V - 4.0 V at different temperatures. (b) The discharge profiles of the Li/LFP cell with the AE electrolyte after the first cycle at different temperatures. (c) The rate capability of the Li/LFP cells with the AE electrolyte solution at different temperatures. (d) The charge and discharge profiles of the Li/LFP cells with the AE electrolyte solution at different rates at 100 °C.

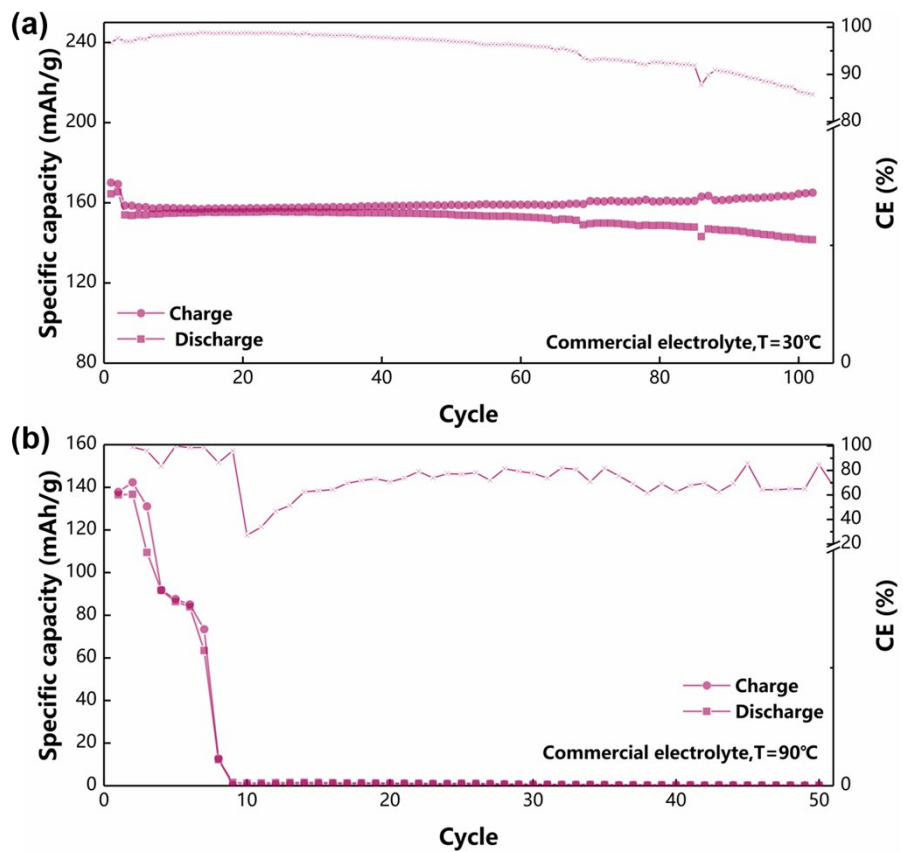


Figure S13. Cycling performance of the Li/LFP cells at 1 C in the voltage range of 2.5 V – 4.0 V with commercial electrolyte solution at (a) 30 °C and (b) 90 °C.

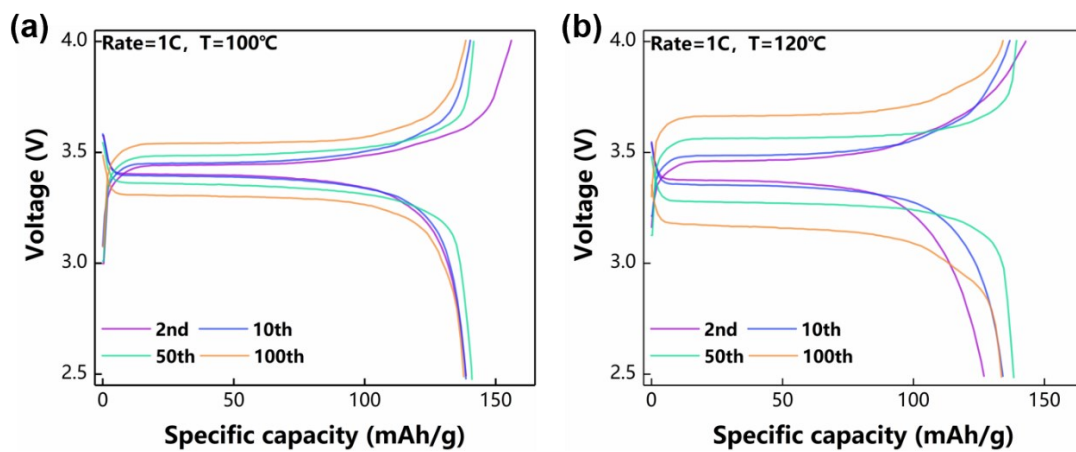


Figure S14. Charge-discharge curves of the Li/LFP cells with the AE co-solvent electrolyte solution after different cycles at (a) 100 °C and (b) 120 °C.

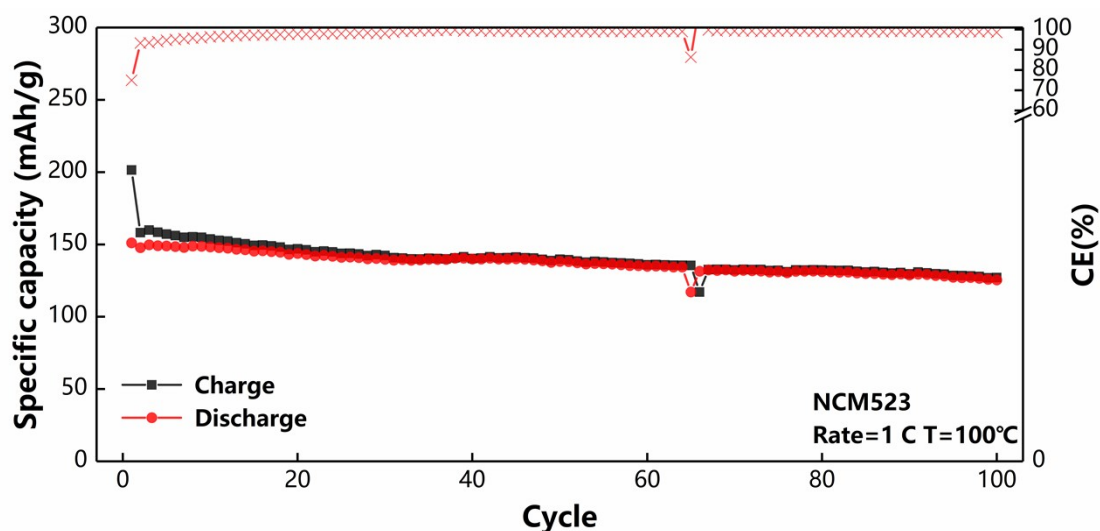


Figure S15. Cycling performance of the Li/NCM523 cells with the AE electrolyte at 1 C in the voltage range of 3.0 V - 4.3 V at 100 °C.

Li/LiFePO₄ (LFP) half-cells are assembled to investigate the temperature-dependent electrochemical performance of the cells with AE electrolytes. As presented in **Figure S12**, Li/LFP half-cells with AE electrolyte exhibit remarkable electrochemical performance in a wide temperature range from 120 °C to -20 °C. At -20 °C and 30 °C, the cells show reversible capacities of 140 mAh/g and 148 mAh/g with the excellent long-term stability of cycling, respectively (**Figure S12a**). The capacity retention ratios are both above 99 % after 100 cycles, achieving average CEs of more than 99.90 % and 99.94 % at -20 °C and 30 °C, respectively. In contrast, the Li metal cell with the commercial electrolytes only possesses the capacity retention ratio of 91.15 % with a continuously reduced CE (**Figure S13a**), because LiPF₆ and linear carbonate like DMC tend to decompose spontaneously at temperatures above 90 °C, which makes the cells only can work 10 cycles (**Figure S13b**). Li/LFP half-cells reveal initial discharge capacities of 152 mAh g⁻¹ and 138 mAh g⁻¹ at 100 °C and 120

°C, respectively. Notably, the Li/LFP cell cycled at 100 °C has a higher initial capacity than 120°C, but after a period of activation, the cell cycled at 120°C still has a higher maximum capacity than 100°C. The maximal capacity of the half-cell cycled at 120 °C is higher than the cell cycled at 100 °C. Moreover, both of capacity loss of cells cycled at 100 °C and 120 °C are observed after reaching a peak, and the capacity retention ratio at 120 °C is lower than that at 100 °C. This originates from a parasitic internal resistance induced at temperatures above 100 °C, which results in an abrupt increase in polarization (**Figure S14**).⁵ The Li/LFP half-cells exhibit reduced CEs values after the first cycle at elevated temperatures after the first cycle, where the capacities do not increase with the increasing temperatures. However, with the temperature drops to -20 °C from 30 °C, the CE value is lowered down from 93.7 % to 77.2 % as shown by **Table S2**. Figure 3b shows discharge curves at -20 °C, 30 °C, 100 °C, 120 °C, and 150 °C. The discharge voltage platforms are almost unchanged when the temperature is lower than 120 °C, and the platform length increases at elevated temperatures. Nevertheless, with the temperature increased to 120 °C, the discharge capacity decreases to 135 mAh/g, owing to the partial destruction of the LFP particles. Moreover, due to the huge polarization of electrodes, the voltage platform drops sharply at 150 °C, reaching only 3.1 V, and the voltage platform length is significantly reduced. The rate performance of the Li/LFP half-cell is displayed in **Figure S12c**. Below 120 °C, the rate performance improves with increasing temperature. At 120 °C, the low-rate (<0.5 C) specific capacity still improves with increasing temperature. But with the current density exceeding 0.5 C, the capacity at 120 °C is lower than that at 100 °C, and

the specific capacity gap is widened with increasing current densities (**Figure S12d**). When the rate is increased to 5 C, the specific capacity is already lower than the cell cycled at 30 °C with the same current density. With the current density further increased to 10 C, the specific capacity is almost zero due to large electrical resistance induced by huge polarization.⁵

Additionally, the Li/NCM523 cell is also assembled to test the long-term performance at 100 °C at high voltage. (**Figure S15**) The cells show an excellent stability which enable capacity retention ratio of 83.4 % with a high average CE of 98.59% at elevated temperature.

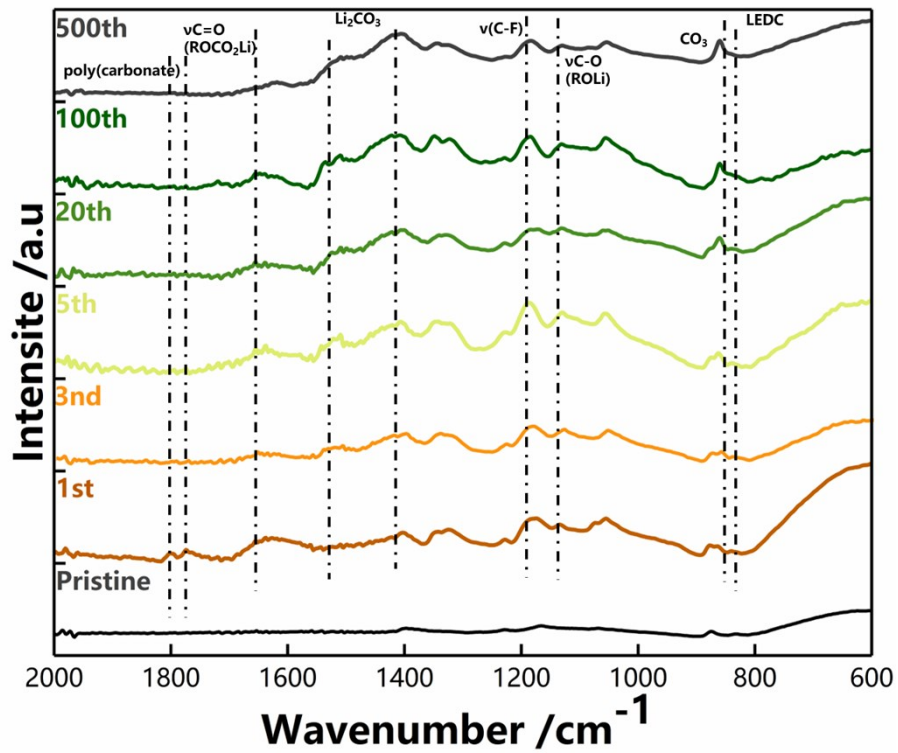


Figure S16. FTIR spectra of the LTO electrode surface cycled with the AE co-solvent electrolyte solution after different cycles.

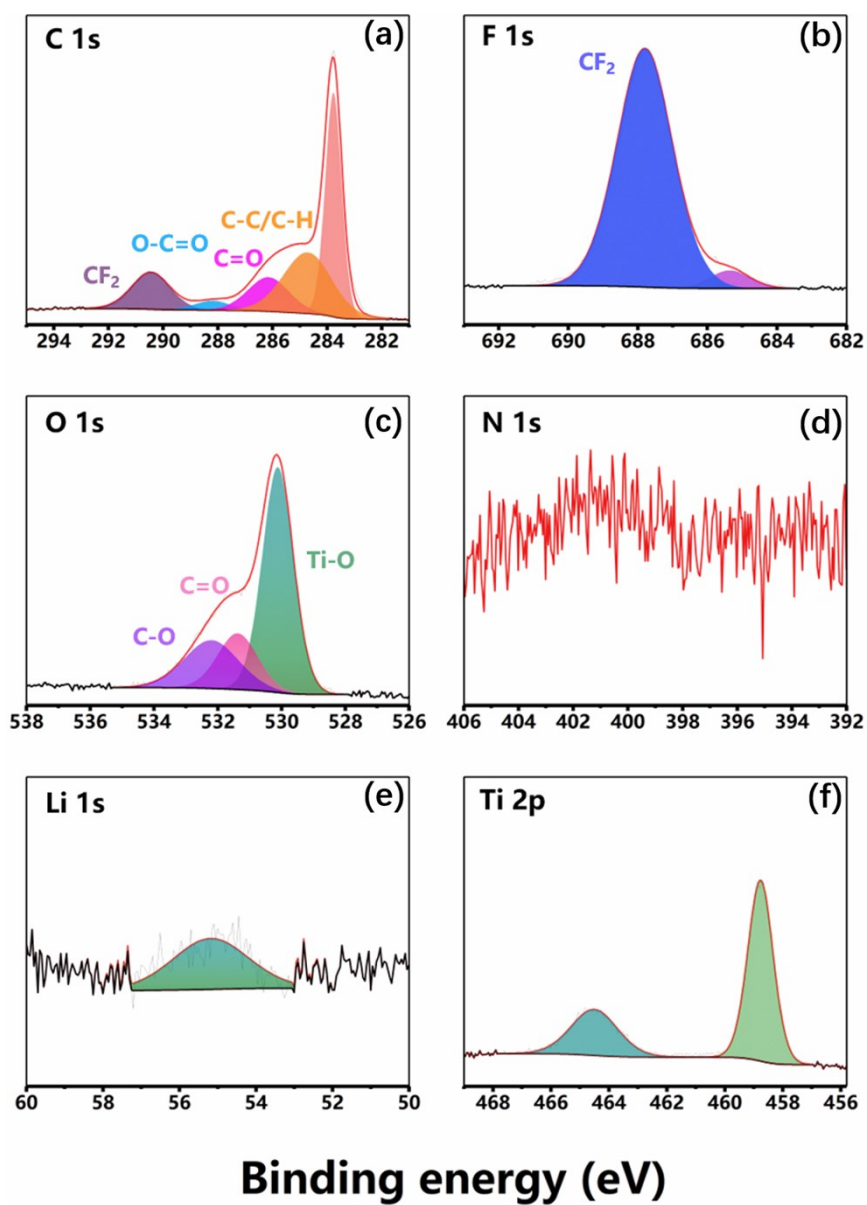


Figure S17. XPS analysis of the pristine LTO electrode.

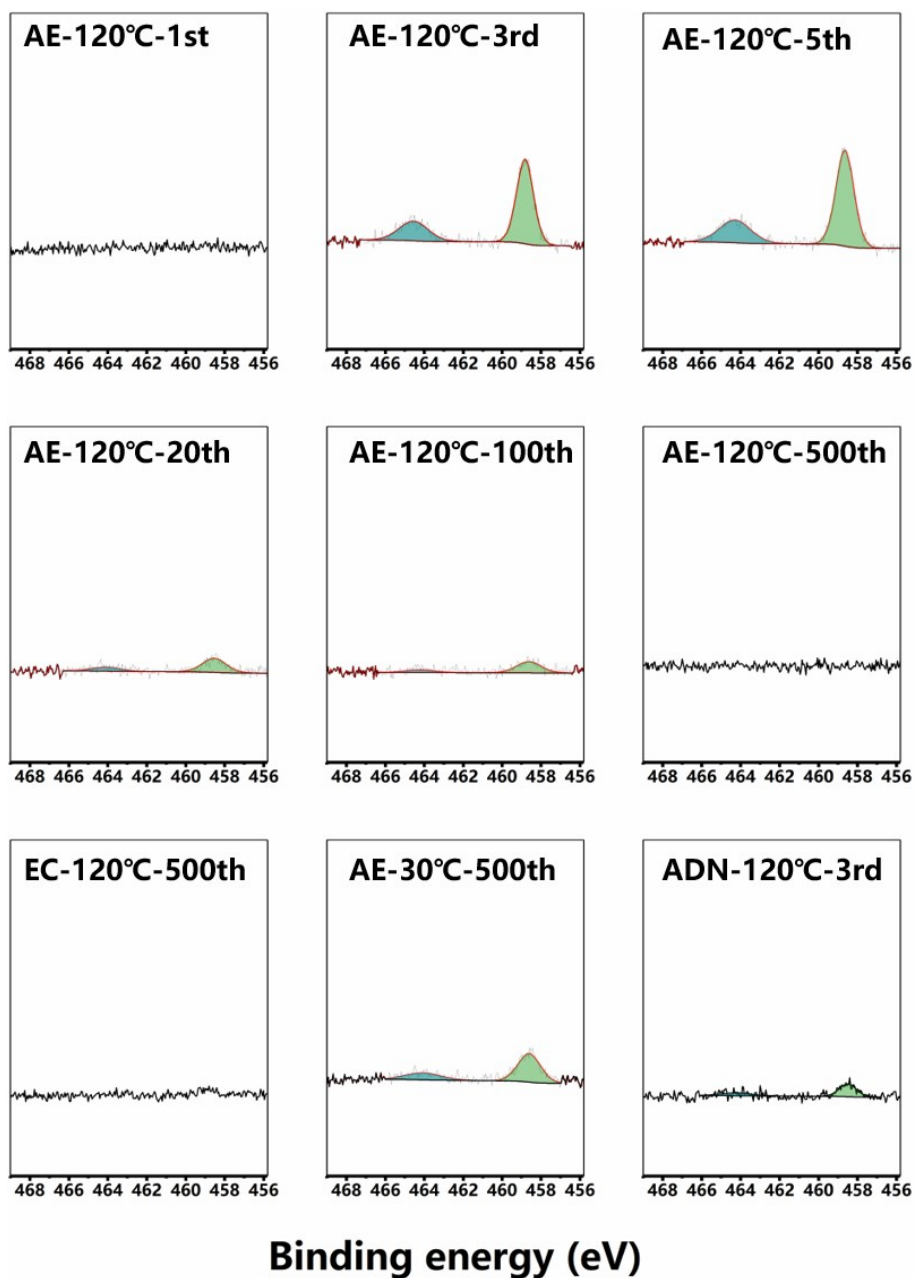


Figure S18. Ti 2p XPS analysis of the LTO electrode cycled under different conditions.

The peak intensity of LTO varies with the thickness of the SEI layer. When the SEI is covered with the active materials, the exposure of LTO is less.

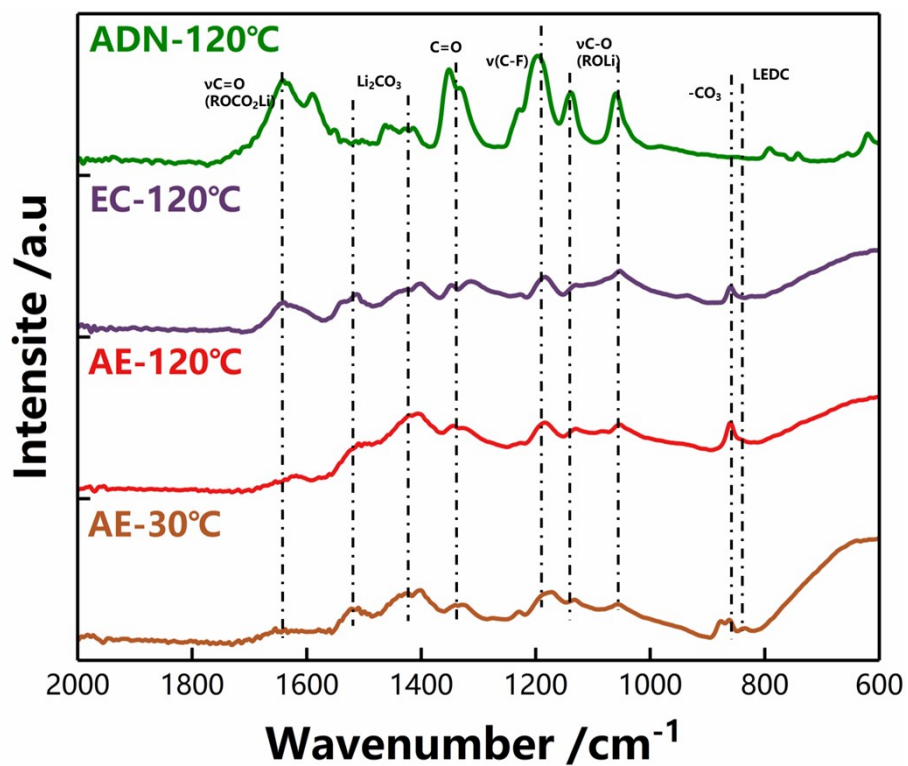


Figure S19. FTIR spectra of the LTO electrode surface cycled under different conditions.

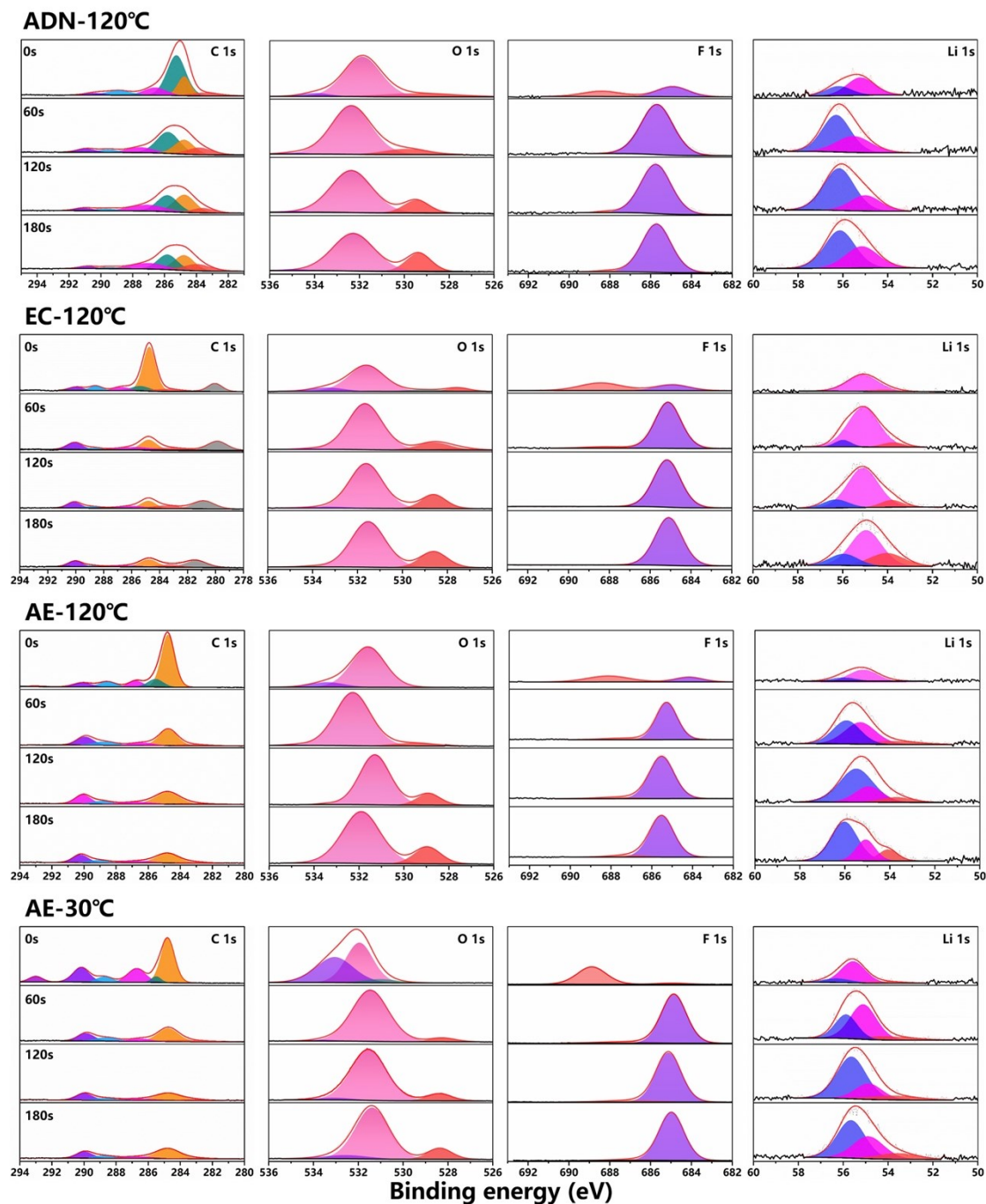


Figure S20. XPS analysis of the SEI layers at the Li metal surface cycled under different conditions. The Li/LTO cell was cycled for 500 cycles (5 C, 1.0 V - 3.0V) and stopped at charge state.

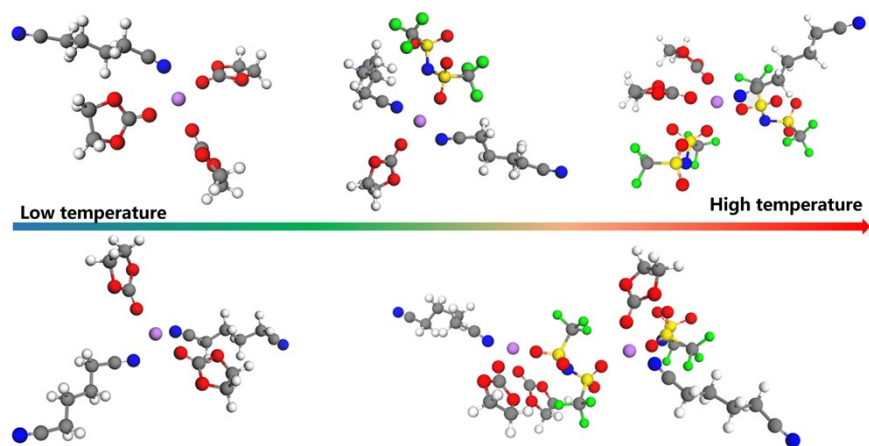


Figure S21. Typical solvated molecule geometrical structures in the AE co-solvent electrolyte solution. Colors for different elements: H-white, Li-purple, C-gray, O-red, F-green, and S-yellow.

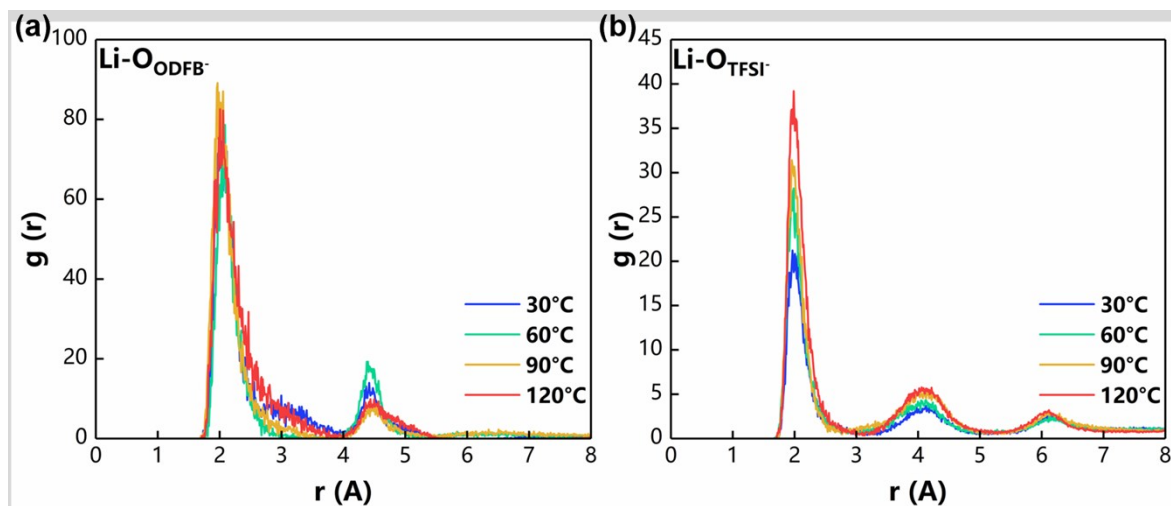


Figure S22. Radial distribution function (RDF) from the MD simulations for the (a) Li-O(ODFB⁻) and (b) Li-O(TFSI⁻).

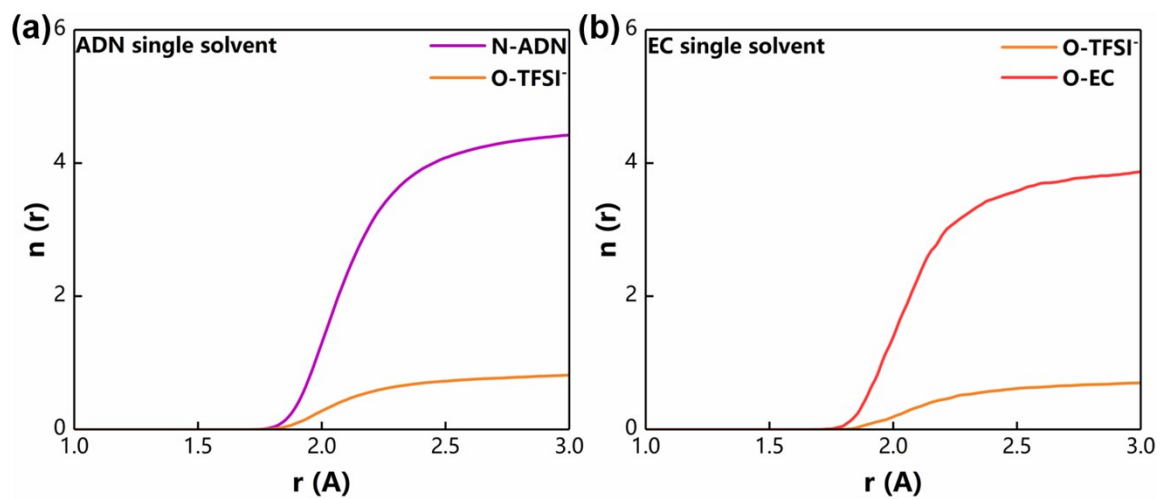


Figure S23. Radial distribution function (RDF) from the MD simulations for the (a) ADN single solvent electrolyte solution and (b) EC single solvent electrolyte solution.

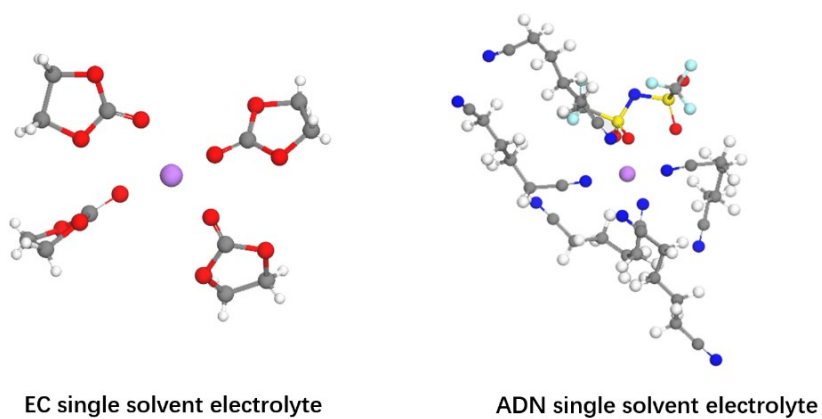


Figure S24. Typical solvated molecule geometrical structures in the EC single solvent electrolyte solution (left) and ADN single solvent electrolyte solution (right) at 120 °C. Colors for different elements: H-white, Li-purple, C-gray, O-red, F-green, and S-yellow.

References

1. Farhat, D.; Ghamouss, F.; Maibach, J.; Edstrom, K.; Lemordant, D., Adiponitrile-Lithium Bis(trimethylsulfonyl)imide Solutions as Alkyl Carbonate-free Electrolytes for Li₄Ti₅O₁₂ (LTO)/LiNi_{1/3}Co_{1/3}Mn_{1/3}O₂ (NMC) Li-Ion Batteries. *Chemphyschem* **2017**, *18*(10), 1333-1344.
2. Farhat, D.; Lemordant, D.; Jacquemin, J.; Ghamouss, F., Alternative Electrolytes for Li-Ion Batteries Using Glutaronitrile and 2-methylglutaronitrile with Lithium Bis(trifluoromethanesulfonyl) Imide. *Journal of the Electrochemical Society* **2019**, *166*(14), A3487-A3495.
3. Ehteshami, N.; Eguia-Barrio, A.; de Meatza, I.; Porcher, W.; Paillard, E., Adiponitrile-based electrolytes for high voltage, graphite-based Li-ion battery. *Journal of Power Sources* **2018**, *397*, 52-58.
4. Geng, Z.; Lu, J. Z.; Li, Q.; Qiu, J. L.; Wang, Y.; Peng, J. Y.; Huang, J.; Li, W. J.; Yu, X. Q.; Li, H., Lithium metal batteries capable of stable operation at elevated temperature. *Energy Storage Materials* **2019**, *23*, 646-652.
5. Kurita, T.; Lu, J. C.; Yaegashi, M.; Yamada, Y.; Nishimura, S.; Tanaka, T.; Uzumaki, T.; Yamada, A., Challenges toward higher temperature operation of LiFePO₄. *Journal of Power Sources* **2012**, *214*, 166-170.